Generation of attosecond coherent X-ray radiation through modulation compression

Ji Qiang [a] & Juhao Wu [b]

[a] Lawrence Berkeley National Laboratory, Berkeley, CA 94720, USA

[b] SLAC National Accelerator Laboratory, Menlo Park, CA 94025, USA

Available online: 04 Jul 2011

First

PLEASE SCROLL DOWN FOR ARTICLE

Generation of attosecond coherent X-ray radiation through modulation compression

Ji Qiang[a]* and Juhao Wu[b]

[a]Lawrence Berkeley National Laboratory, Berkeley, CA 94720, USA; [b]SLAC National Accelerator Laboratory, Menlo Park, CA 94025, USA

In this paper, we propose a scheme to generate tunable attosecond coherent X-ray radiation for future light source applications. This scheme uses a short-pulse seeding laser, two bunch compressors, and a laser chirper to generate a prebunched, kilo-Ampere current electron beam from an initial 10-Ampere low-current electron beam. Such an electron beam sent into a short undulator generates attosecond coherent soft X-ray radiation. The final X-ray radiation wavelength can be tuned by adjusting the compression factor. It also allows one to control the final radiation pulse length by controlling the seeding laser pulse length or the compression factor. As an illustration, we present an example to generate 1 GW, 200 attosecond, 1 nm coherent X-ray radiation from a 28 A current, 200 nm laser modulated beam.

Keywords: modulation compression; attosecond radiation; X-ray radiation

1. Introduction

Ultra-short coherent X-ray sources have important applications in biology, chemistry, condensed matter physics, and material science. In recent years, there has been growing interest in generating single attosecond X-ray radiation using Free Electron Lasers (FELs) [1–8]. In our previous study, a modulation compression scheme was proposed to compress the initial seeding laser modulation to generate short-wavelength X-ray radiation [9].[1] That scheme consisted of a modulator, a chirper, a bunch compressor, another chirper, and another bunch compressor. In order to effectively chirp and de-chirp the modulated electron beam, two laser modulators besides the initial seeding laser were used as chirpers before the two bunch compressors. The fluctuation of the field amplitude in the first chirping laser will cause fluctuation of the electron beam energy chirp. For a large compression factor, e.g. 100, a small change of the electron beam energy chirp will cause a large change of the compression factor and hence the compressed beam current. To overcome this large jittering effect, we recently proposed a new scheme to compress the initial seeding modulation to generate short-wavelength radiation [12]. A schematic plot of the lattice layout of the scheme is given in Figure 1.

It consists of an energy chirped electron beam, a seeding laser modulator, a bunch compressor A, a laser chirper, and another bunch compressor B. The scheme uses a chirped electron beam as an input to the seeding laser modulator. The requirement of the compression factor from the first bunch compressor is also reduced from the order of 100 to the order of 10. This significantly reduces the final current fluctuation due to the effects of the jitter of the electron energy chirp. It also makes the scheme more compact compared with the previous scheme, in reference [9]. In that scheme, an example was given to generate attosecond coherent X-ray radiation using a few-cycle laser chirper. Here, the laser chirper denotes a laser modulator that is used to introduce local energy chirp to an electron beam. The electron beam bunch length after the first bunch compressor is longer than the laser chirper wavelength. Only a periodic segment of the beam is compressed correctly. In this study, we explore a situation where the bunch length after the first bunch compressor is less than the laser chirper wavelength. In this case, a major part of the beam is compressed. The requirement of the initial current can be even lower due to the large beam current compression factor (on the order of 100). Instead of using a few-cycle laser chirper, in this study, a short-pulse seeding laser before the first bunch compressor is used to generate the final attosecond X-ray radiation. This makes the final radiation pulse length easily tunable by controlling the seeding laser pulse length or the compression factor. In comparison with other proposed schemes in references [1–8], the scheme proposed in this paper has the advantage of generating more than 1 GW of coherent attosecond X-ray radiation using a much

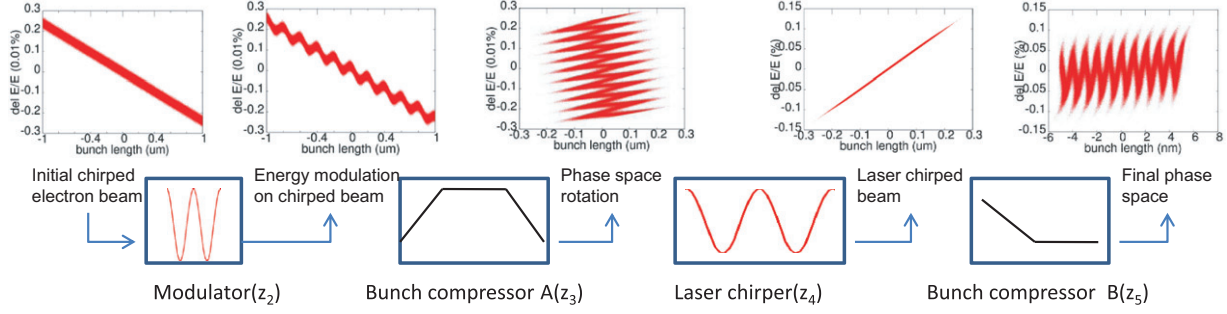*Corresponding author. Email: jqiang@lbl.gov

Figure 1. A schematic plot of the lattice layout of the modulation compression scheme together with longitudinal phase space distribution of an electron beam after each lattice element. (Note the changes of the vertical axis scale in the laser-chirped beam and the horizontal axis scale in the final phase space.) (The color version of this figure is included in the online version of the journal.)

lower current electron beam (order of 10-Amperes instead of kilo-Amperes).

The organization of this paper is as follows: after the introduction in Section 1, the seeding laser modulation of a chirped electron beam will be discussed in Section 2; the modulation compression scheme is presented in Section 3; an example of generating a coherent attosecond X-ray radiation is presented in Section 4; and the final discussions are given in Section 5.

2. Laser modulation of a chirped beam

In the scheme used in this study, an energy chirped electron beam is sent into the seeding laser modulator to obtain initial energy modulation. By applying the energy chirping first instead of energy modulation first, it avoids the potential modulation distortion from the collective effects during the process of chirping inside the linac. This also allows one to use the full linac to generate the initial energy-bunch length chirp. Notice that, in most of the currently operating XFELs and those under design, the residual energy chirp after the bunch compression has to be removed by running the electron bunch off crest after the bunch compressor. That makes the acceleration less efficient. Furthermore, inserting a chicane with a reasonable compression factor inside such a linac will produce the same amount of chirp required in this compression scheme and will reduce the total voltage needed from the linac by a factor of that compression factor. For an electron with initial longitudinal coordinates (z_0, δ_0) before chirping, where z is the relative longitudinal distance with respect to the center reference particle, and $\delta = \Delta E/E$ is the relative energy spread, the longitudinal coordinates after the chirping and the first laser modulation will be:

$$z_2 = z_0 \qquad (1)$$

$$\delta_2 = \delta_1 + A \frac{1}{1+\delta_1} \frac{\sin(4N_w\delta_1\pi)}{4N_w\delta_1\pi} \sin(kz) \qquad (2)$$

where $\delta_1 = \delta_0 + h\,z$ represents the relative energy spread after the chirping from a linac with h standing for the energy chirp, A is the modulation amplitude in the unit of the relative energy, N_w is the number of periods of the wiggler used in the laser modulator, and k is the wave number of the seeding laser. Given the fact that the bunch length is normally below a millimeter, the required initial chirp for the first bunch compressor is on the order of tens m^{-1}, and a small number of wiggler periods, Equation (2) can be approximated as [13]

$$\delta_2 = \delta_1 + A \sin(kz). \qquad (3)$$

This is the same equation for an electron with the laser modulation first and then the chirping second as used in the previous compression scheme.

To check the laser modulation of a chirped beam, we also did numerical simulation of a section of a chirped electron beam passing through a Gaussian laser field and a wiggler field inside a modulator. Here, we assumed an electron beam with an energy of 2 GeV and an energy chirp of $-24.7\,m^{-1}$ entering a laser modulator with five wiggler periods (7.0 cm period length), 2 Tesla magnetic field, and 440 kW laser power. Figure 2 shows the longitudinal phase space distribution of such an initially chirped beam at the end of the modulator together with the phase space distribution of an initially modulated beam at the end of the linear chirper.

It is seen that the two longitudinal phase space distributions with and without initial energy chirp are very close to each other. This suggests that the energy deviation from the resonant energy of the chirped electrons does not have a significant effect on the initial
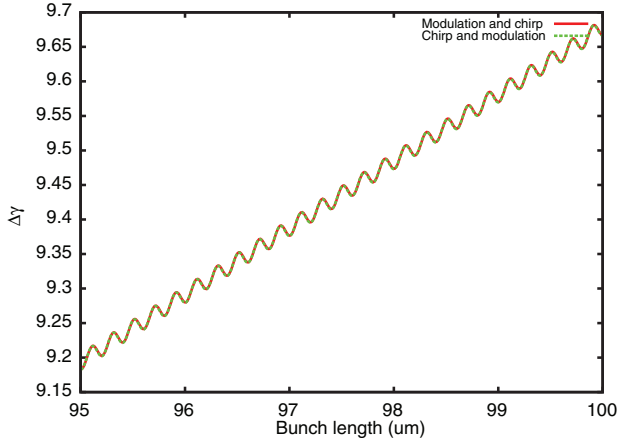
Figure 2. Longitudinal phase space distribution for an initially chirped beam at the end of the modulator (green) and an initially modulated beam at the end of the chirper (red). (The color version of this figure is included in the online version of the journal.)

energy modulation as predicted from Equation (3). This is due to the fact that laser electron resonant interaction inside a short wiggler has a large bandwidth. Such a bandwidth allows the chirped electrons to get nearly the same energy modulation as the electrons without initial energy chirp.

3. Modulation compression scheme

In the following, we will derive the longitudinal phase space distribution of the beam transported through an ideal lattice as shown in Figure 1 using a one-dimensional model. The beam is assumed to be longitudinally frozen in most of the lattice except in the bunch compressors. The initial longitudinal phase space distribution function before the laser modulator is given as:

$$f(z_0, \delta_0) = F(z_0, (\delta_0 - h\, z)/\sigma) \quad (4)$$

where z_0 is the longitudinal coordinate with respect to the bunch center, $\delta_0 = \Delta E_0/E_0$ is the relative energy deviation, σ is a constant related to the initial energy spread. After the laser modulator, the distribution function becomes

$$f(z_2, \delta_2) = F\left(z_2, \frac{\delta_2 - hz_2 - A\sin(kz_2)}{\sigma}\right). \quad (5)$$

Next, the beam passes through the bunch compressor A. The longitudinal coordinate becomes, $z_3 = z_2 + R_{56}^a\delta_2$, where R_{56}^a is the momentum compaction factor of the bunch compressor A.

After the bunch compressor, the phase space distribution becomes

$$f_3(z_3, \delta_3) = F\Bigg(z_3 - R_{56}^a\delta_3,$$
$$\frac{\delta_3 - hCz_3 - CA\sin(k(z_3 - R_{56}^a\delta_3))}{C\sigma}\Bigg) \quad (6)$$

where $C = 1/(1 + R_{56}^a h)$ is the bunch compression factor of the first bunch compressor A. Then the beam is transported through the chirper B that will introduce another energy-bunch length correlation, $\delta_4 = \delta_3 + h_b\, z_3$, where h_b is the energy chirp across the bunch length of the beam caused by the second chirper. After the chirper B, the phase space distribution becomes

$$f_4(z_4, \delta_4) = F\Bigg(z_4(1 + R_{56}^a h_b) - R_{56}^a\delta_4,$$
$$\frac{\left\{\begin{array}{l}\delta_4 - (h_b + hC)z_4 \\ -CA\sin(k(z_4(1 + R_{56}^a h_b) - R_{56}^a\delta_4))\end{array}\right\}}{C\sigma}\Bigg). \quad (7)$$

Finally the beam is transported through the second bunch compressor B. The longitudinal coordinate of the beam becomes, $z_5 = z_4 + R_{56}^b\delta_4$, where R_{56}^b is the momentum compaction factor of the bunch compressor B. The final longitudinal phase space distribution becomes

$$f(z, \delta) = F(Mz - (R_{56}^b M + R_{56}^a)\delta, [\delta(1 + hR_{56}^a + (h_b + hM)R_{56}^b) - (h_b + hM)z - A\sin(kMz - k(R_{56}^b M + R_{56}^a)\delta)]/\sigma) \quad (8)$$

where

$$M = 1 + h_b R_{56}^a \quad (9)$$

denotes the final modulation compression factor. If the second bunch compressor B is set up so that

$$R_{56}^b = -R_{56}^a/M \quad (10)$$

the final longitudinal distribution function can be written as

$$f(z, \delta) = F\left(Mz, \frac{\delta - (h_b + hM)Mz - MA\sin(kMz)}{M\sigma}\right). \quad (11)$$

If the chirp h_b introduced by the laser chirper is $-hC$, i.e. $h_b = -hC$, the total modulation compression factor

M will be C, i.e. $M = C$. The final longitudinal distribution function will be

$$f(z, \delta) = F\left(Cz, \frac{\delta - CA\sin(kCz)}{C\sigma}\right). \qquad (12)$$

From the above distribution, we see that the longitudinal modulation wavelength is compressed by a factor of C and the relative amplitude of modulation is increased by a factor of C. If the beam is over de-chirped inside the laser chirper, i.e. $h_b = (-h + \tilde{h})C$, the total modulation compression factor will be $M = (1 + \tilde{h}R_{56}^a)C$. Here, the over de-chirp means that the energy chirp from the laser chirper not only undoes the previous energy chirp of the beam after the compression but also introduces extra energy chirp in the opposite direction with respect to the previous chirp. This improves the final compression factor in the scheme by a factor of $1 + \tilde{h}R_{56}^a$, where the $\tilde{h}$ stands for the extent of over de-chirping of the initial chirp through the laser chirper. The final longitudinal distribution function will be

$$f(z, \delta) = F\left(Mz, \frac{\delta - M\tilde{h}z - MA\sin(kMz)}{M\sigma}\right). \qquad (13)$$

The above distribution function represents a compressed modulation in a chirped beam. It should be noted that the momentum compaction factor of the second bunch compressor B does not have to be of the opposite sign with respect to the first bunch compressor A if the total compression factor M, i.e. C or $1 + \tilde{h}R_{56}^a$, is made negative. In the above equations, we have also assumed a linear laser chirper instead of the real sinusoidal function from the laser modulator. The effects of sinusoidal energy modulation from the laser chirper will be discussed below. Assume an initial uniform current distribution and a Gaussian energy distribution in function F of the Equation (4), the final current distribution can be represented as a Fourier series yielding [14]:

$$I(z) = I_0\left(1 + 2\sum_{n=1}^{\infty} b_n \cos(nK_n z)\right) \qquad (14)$$

where

$$K_n = \frac{k}{1 + hR_{56}^a + (h_b + hM)R_{56}^b} \qquad (15)$$

is the compressed current modulation wave number and the coefficient b_n (i.e. bunching factor of harmonic n) is given as:

$$b_n = J_n(-nD_A k)\exp\left(-\frac{1}{2}n^2k^2 D_B^2\right) \qquad (16)$$

where the J_n is the Bessel function of order n, $D_A = A(R_{56}^a + R_{56}^b M)/(1 + hR_{56}^a + (h_b + hM)R_{56}^b)$, and $D_B = \sigma(R_{56}^a + R_{56}^b M)/(1 + hR_{56}^a + (h_b + hM)R_{56}^b)$. Under the

condition $R_{56}^b = -R_{56}^a/M$ proposed in this paper, $K_n = Mk$. For small jitters of the relative initial beam energy chirp $\tilde{h}_a$ and the chirp $\tilde{h}_b$, the jitter of the compressed current modulation wave number is given as:

$$\delta K_n/K_n = (R_{56}^a h_b/C)\,\tilde{h}_b + hR_{56}^a h_b R_{56}^a\,\tilde{h}_a\tilde{h}_b. \qquad (17)$$

It is seen that the final compressed current modulation wave number is less sensitive to the initial beam energy chirper jitter than to the laser chirper jitter. It should be noted that the bunching factor under the ideal nominal parameter setting of the R_{56}^b will be zero. This corresponds to the compressed phase space energy modulation of a chirped beam. By detuning the R_{56}^b from the nominal value, a large current bunching factor can be obtained for the compressed modulation at the fundamental mode.

It is easy to produce a large energy chirping amplitude inside the chirper after the first bunch compressor using a conventional RF linac structure. However, using a laser modulator, this chirp can be easily achieved by taking advantage of the short wavelength and the high power of the laser. The disadvantage of using such a laser chirper is that, depending on the beam bunch length and the laser chirper wavelength, the whole of the electron beam might not be linearly chirped owing to the sinusoidal form of the energy modulation.

4. Attosecond X-ray radiation generation using a short-pulse seeding laser

In this section, we show an example for generating attosecond coherent X-ray radiation using a short-pulse seeding laser in above compression scheme. A short-bunch electron beam (e.g. 100 μm) with 9.16 pC charge, 2 GeV energy, $-23.95\,\text{m}^{-1}$ energy chirp, and a slice energy spread of 1×10^{-6} is assumed at the beginning of the laser modulator. This energy spread is based on an assumption of 2 keV uncorrelated energy spread inside a beam coming out of a photoinjector. A few keV energy spread was observed at the LCLS photoinjector experiment [15]. The initial relative energy modulation amplitude is $A = 2 \times 10^{-6}$. Only a fraction of the electron beam is energy modulated by a short-pulse laser with a modulation width around 30 fs. After the modulator, we add a slice energy spread of 0.54 keV to account for the synchrotron radiation effects inside the wiggler magnet using an estimate from references [16,8]. After the beam goes through the modulator, it passes through a standard C shape chicane bunch compressor. Here, we have assumed that the R_{56} of the chicane is about 4 cm. As the electron beam passes through a bending

magnet, the quantum fluctuation of the incoherent synchrotron radiation causes the increase of the uncorrelated energy spread. Here, we assumed four 4 m long bending magnets inside the chicane each with 0.052 radian bending angle in order to reduce the increase of the uncorrelated energy spread. The uncorrelated rms energy spread $\Delta\sigma_E$ induced by the incoherent synchrotron radiation inside a bending magnet can be estimated from [17]

$$\Delta\sigma_E = \frac{E}{L}\sqrt{\frac{55}{24\sqrt{3}}\frac{r_e^2}{\alpha}\gamma^5\theta^3} \qquad (18)$$

where L is the length of the bending magnet, r_e is the classical electron radius, α is the fine structure constant, γ is the relativistic factor of the beam, θ is the bending angle of the magnet. Using above assumed magnet parameters, this gives about 0.44 keV increase of the uncorrelated energy spread after the first bunch compressor chicane. The effects of coherent synchrotron radiation are not included in this study due to the assumption of the low current (28 Ampere) beam. The microbunching effects from the coherent synchrotron radiation and other collective effects will be weak. After the beam passes through this bunch compressor, the total bunch length of the beam is compressed down to about 4 μm with a compression factor of 25. This beam is transported through another laser modulator with 10 μm resonant wavelength. Since the modulation wavelength is longer than the bunch length, this modulator works as a laser chirper to remove the global energy chirp across the beam. Another 0.54 keV increment of uncorrelated energy spread is added to the beam due to the synchrotron radiation effects inside the wiggler. After the beam transports through the laser chirper, it passes through a dog-leg type bunch compressor that can provide opposite sign R_{56} compared with the first bunch compressor. The required R_{56} from this bunch compressor is a factor of M smaller than that of the first bunch compressor. For a total final compression factor of 200 through the system, the R_{56} of the second bunch compressor is about 0.2 mm. Figure 3 shows the longitudinal phase space of the beam at the end of the second bunch compressor.

It is seen that after the second bunch compressor, the initial 30 fs modulated beam is compressed to a width about 150 attoseconds. The initial uncorrelated rms energy spread of 1×10^{-6} has risen to about 2×10^{-4} with a correlated energy chirp. This energy spread is still small enough for generating coherent X-ray radiation in an undulator downstream. Figure 4 shows the projected current distribution for this prebunched beam.
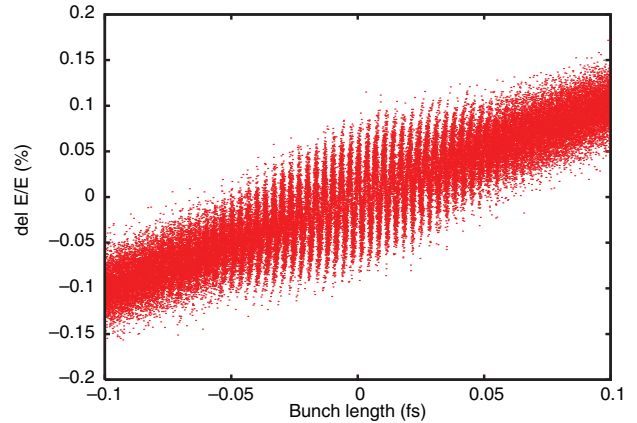

Figure 3. Longitudinal phase space at the end of the bunch compression scheme. (The color version of this figure is included in the online version of the journal.)
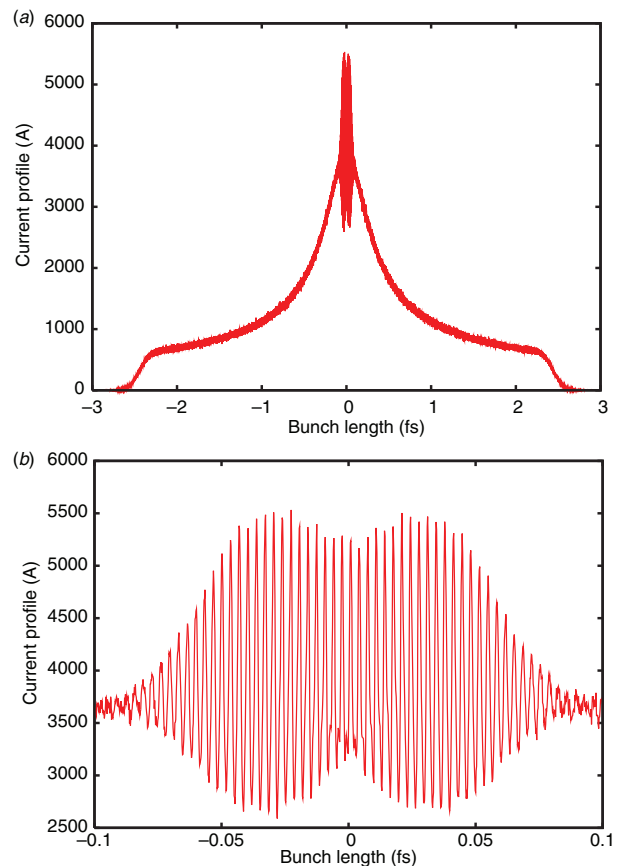

Figure 4. Beam current distribution after the compression scheme (*a*) and the zoom-in current distribution around the center of the beam (*b*). (The color version of this figure is included in the online version of the journal.)

Given the initial 28 A current, the central prebunched current peak with 1 nm wavelength modulation reaches 5.5 kA after the above compression scheme. Such a highly prebunched beam can be used to

generate coherent attosecond X-ray radiation through a short undulator.

Two laser modulators, one for initial energy modulation seeding and the other for global correlated energy de-chirping, are used in this scheme for attosecond generation. Figure 5 shows the relative energy modulation from the seeding laser and from the laser chirper.

The modulation amplitude required from the seeding laser is small due to the compression amplification. Assuming 1 Tesla wiggler magnet field, the required 200 nm laser power is about 0.35 MW with a wiggler length of 33 cm and a period of 11 cm. The modulation amplitude from the laser chirper is relatively large in order to de-chirp the amplified initial energy chirp. Assuming 1 Tesla magnetic field, it requires about 31 GW laser power inside a 1.2 m long wiggler with a period of about 40 cm. The energy spread induced by synchrotron radiation inside the wiggler can be estimated following [8,16]

$$\Delta\sigma_E = E\sqrt{4.16\frac{r_e^2}{\alpha}\gamma^2 N_w\left(\frac{eB}{mc}\right)^2} \qquad (19)$$

where N_w is the number of wiggler periods and B is the wiggler magnetic field. This gives about 0.54 keV increase of the uncorrelated energy spread after the laser modulator and the laser chirper. The transverse profile effects of the modulating laser were not included in the study, assuming that the transverse spot size of the laser beam is much larger than that of the electron beam.

To study the detailed radiation process and the radiation properties, we used the GENESIS simulation code [18] to calculate the coherent X-ray radiation through a short undulator radiator. The electron particle distribution from the above-mentioned one-dimensional simulation is used for the GENESIS simulation. The normalized emittance of the electron beam is chosen to be 0.2 μm. The transverse distribution of the beam is assumed as a Gaussian distribution with 12.4 μm and 11.4 μm rms size in horizontal and vertical direction, respectively. The length of the radiator is 1.5 m with an undulator period of 1.5 cm.

The details of the radiation properties at the end of the undulator are shown in Figure 6, where the radiation pulse power temporal profile is shown as the left subplot and the radiation pulse spectral profile is shown as the right subplot. The profiles are fit to Gaussian curves, which give a temporal rms size of 86 attoseconds and a spectral rms width of 4.1 pm. This results in a time-bandwidth product (the angular frequency rms width times the time rms width of the radiation) of about 0.65, which is close to the transform limit of the X-ray pulse. The full width at
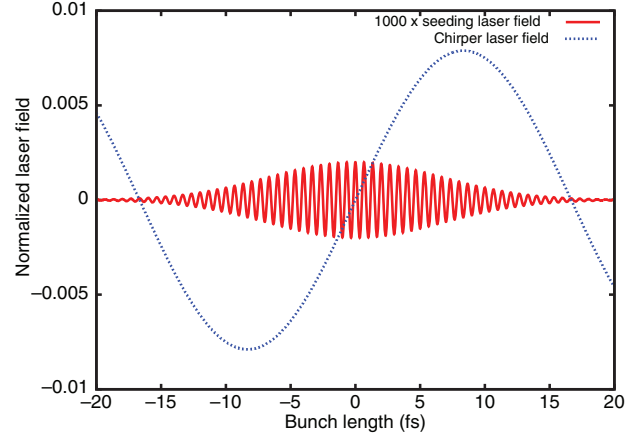

Figure 5. Relative energy modulation from the seeding laser and the laser chirper. (The color version of this figure is included in the online version of the journal.)
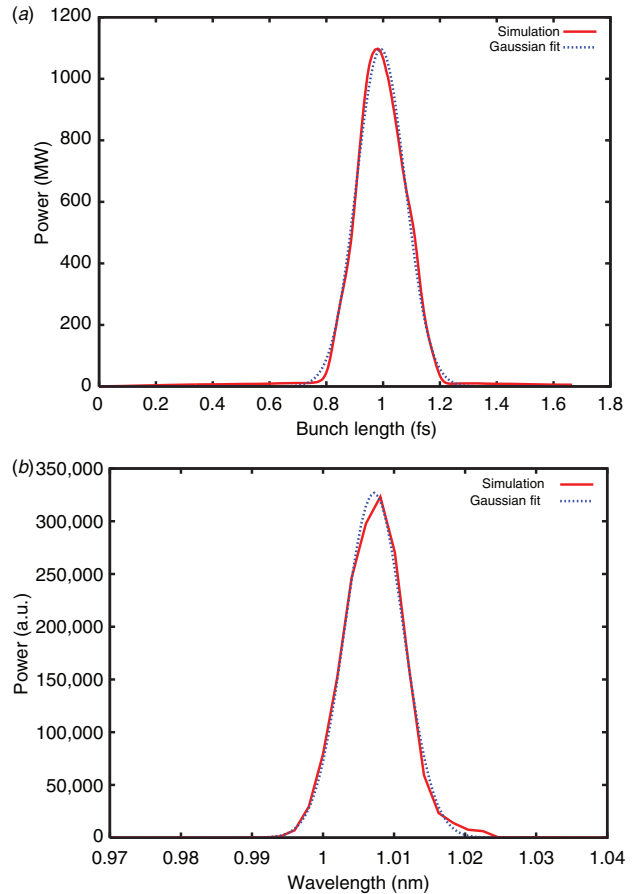

Figure 6. The radiation pulse temporal profile (*a*) at the end of the 1.5 m long undulator and the radiation pulse spectral profile (*b*) at the end of the 1.5 m long undulator. (The color version of this figure is included in the online version of the journal.)

half maximum of the radiation pulse is about 205 attoseconds, which is larger than the width of the central modulated current density distribution. This is due to the slippage of the photon pulse with respect to the electron bunch inside the radiator. In summary, in the above example, a single 1 nm, 200 attosecond, 1 GW peak power X-ray radiation was generated with a 28 A current electron beam seeded by a 200 nm laser.

5. Discussion

In this paper we proposed generating attosecond coherent X-ray radiation using a modulation compression scheme. This scheme allows one to tune the final X-ray radiation wavelength by adjusting the compression factor. It also allows one to control the final radiation pulse length by controlling the seeding laser pulse length or the compression factor. The high compression factor in the proposed scheme also lowers the required initial current in order to achieve a final kilo-Ampere electron beam current. This helps maintain good beam quality transporting through the linear accelerator.

The proposed scheme requires a small initial seeding laser power due to the compression amplification. This makes it possible to use a relatively lower power ($\sim$100 kW) and a shorter wavelength laser ($\sim$10 nm) from the higher-order harmonic generation (HHG) scheme to seed the electron beam before the first bunch compressor [19]. This could result in a prebunched beam with a modulation wavelength down to the hard X-ray regime using the above single stage compression scheme. Such a prebunched beam can be used to generate coherent attosecond hard X-ray radiation for applications such as core electron ultrafast dynamics studies [20]. Careful lattice design is needed in order to preserve the prebunched microstructure of the electron beam before entering the undulator for X-ray radiation [21].

There also exist some potential technical challenges associated with this scheme. These include synchronization between the electron beam, the seeding laser, and the laser chirper, and the stability of the laser field. For example, the energy jitter of the chirped beam at the entrance of the first bunch compressor results in the time jitter of the beam. Those challenges might be solved in the future with the rapid advance of the laser technology and the electron beam instrumentation technology [22,23]. Using a combination of feedback control and nonlinear optical limiter technology, the fluctuation of the laser field might be controlled within the tenth percentage level [24]. Recently, a lot of progress has been made to synchronize the electron beam and the laser beam for FEL-based light sources. Experimental results have demonstrated the synchronization between the electron beam and the laser beam on the level of 10 fs [25]. Further development of laser electron beam synchronization by using a master laser to lock the whole accelerator system, including the photo-electron driving laser, RF cavity, and modulation lasers, might be able to push the laser-electron beam synchronization within the order of subfemtoseconds [26].

Note

1. A similar scheme using accelerator chirpers was also independently proposed by Ratner et al. [10,11].

References

[1] Zholents, A.A.; Fawley, W.M. *Phys. Rev. Lett.* **2004,** *92,* 224801.
[2] Zholents, A.A.; Penn, G. *Phys. Rev. Spec. Top.–Accel. Beams* **2005,** *8,* 050704.
[3] Saldin, E.L.; Schneidmiller, E.A.; Yurkov, M.V. *Phys. Rev. Spec. Top.– Accel. Beams* **2006,** *9,* 050702.
[4] Wu, J.; Bolton, P.R.; Murphy, J.B.; Wang, K. *Opt. Express* **2007,** *15,* 12749.
[5] Zholents, A.A.; Zolotorev, M.S. *New J. Phys.* **2008,** *10,* 025005.
[6] Ding, Y.; Huang, Z.; Ratner, D.; Bucksbaum, P.; Merdji, H. *Phys. Rev. Spec. Top.–Accel. Beams* **2009,** *12,* 060703.
[7] Xiang, D.; Huang, Z.; Stupakov, G. *Phys. Rev. Spec. Top.–Accel. Beams* **2009,** *12,* 060701.
[8] Zholents, A.A.; Penn, G. *Nucl. Instrum. Methods A* **2010,** *612,* 254–259.
[9] Qiang, J. *Nucl. Instrum. Methods A* **2010,** *621,* 39.
[10] Ratner, D.; Huang, Z.; Chao, A. Presented at the 31st International Free Electron Laser Conference, Liverpool, UK, August 23–28, 2009.
[11] Ratner, D.; Huang, Z.; Chao, A. *Phys. Rev. Spec. Top.–Accel. Beams* **2011,** *14,* 020701.
[12] Qiang, J.; Wu, J. *Nucl. Instrum. Methods A* **2011**, *640,* 228–231.

[13] Zholent, A.A.; Holldack, K. Presented at the Free Electron Laser Conference, Berlin, 2006; Paper THPPH059.

[14] Yu, L. *Phys. Rev. A* **1991**, *44,* 5178–5193.

[15] Akre, R.; Dowell, D.; Emma, P.; Frisch, J.; Gillevich, S.; Hays, G.; Hering, V.; Iverson, V.; Limborg-Deprey, C.; Loos, H.; Miahnahri, A.; Schmerge, J.; Turner, J.; Welch, J.; White, V.; Wu, J. *Phys. Rev. Spec. Top.– Accel. Beams* **2008,** *11,* 030703.

[16] Saldin, E.; Schneidmiller, E.; Yurkov, M. *Nucl. Instrum. Methods A* **1996**, *381,* 545–547.

[17] Jowett, J.M. *Introductory Statistical Mechanics for Electron Storage Rings*, SLAC-PUB-4033, July 1986.

[18] Reiche, S. *Nucl. Instrum. Methods A* **1999**, *429,* 243–248.

[19] Takahashi, E.J.; Nabekawa, Y.; Midorikawa, K. *Appl. Phys. Lett*. **2004**, *84,* 4.

[20] Bergmann, U.; Corlett, J.; Dierker, S.; Falcone, R.; Galayda, J.; Gibson, M.; Hastings, J.; Hettel, B.; Hill, J.; Hussain, Z.; Kao, C.; Kirz, J.; Long, G.; McCurdy, B.;

Raubenheimer, T.; Sannibale, F.; Seeman, J.; Shen, Z.-X.; Shenoy, G.; Schoenlein, B.; Shen, Q.; Stephenson, B.; Stöhr, J.; Zholents, A. *Science and Technology of Future Light Sources*; White Paper, LBNL-1090E-2009: February 2009.

[21] Li, Y.; Decking, W.; Faatz, B.; Pflueger, J. *Phys. Rev. Spec. Top.–Accel. Beams* **2010,** *13,* 080705.

[22] Carlsten, B.E.; Colby, E.R.; Esarey, E.H.; Hogan, M.; Kärtner, F.X.; Graves, W.S.; Leemans, W.P.; Rao, T.; Rosenzweig, J.B.; Schroeder, C.B.; Sutter, D.; White, W.E. *Nucl. Instrum. Methods A* **2010,** *622,* 657.

[23] Byrd, J.M.; Shea, T.J.; Denes, P.; Siddons, P.; Attwood, D.; Kaertner, F.; Moog, L.; Li, Y.; Sakdinawat, A.; Schlueter, R. *Nucl. Instrum. Methods A* **2010,** *623,* 910–920.

[24] Wilcox, R. Private communication, 2010.

[25] Wilcox, R.; Byrd, J.M.; Doolittle, L.; Huang, G.; Staples, J.W. *Opt. Lett.* **2009,** *34,* 3050–3052.

[26] Byrd, J.M. Private communication, 2011.